Spin-flop transition in uniaxial antiferromagnets: magnetic phases, reorientation effects, multidomain states

A.N. Bogdanov[1,2],* A.V. Zhuravlev[2], and U.K. Rößler[1†]
[1]*IFW Dresden, Postfach 270116, D-01171 Dresden, Germany and*
[2]*Donetsk Institute for Physics and Technology, 340114 Donetsk, Ukraine*
(Dated: February 6, 2008)

The classical spin-flop is the field-driven first-order reorientation transition in easy-axis antiferromagnets. A comprehensive phenomenological theory of easy-axis antiferromagnets displaying spin-flops is developed. It is shown how the hierarchy of magnetic coupling strengths in these antiferromagnets causes a strongly pronounced *two-scale* character in their magnetic phase structure. In contrast to the major part of the magnetic phase diagram, these antiferromagnets near the spin-flop region are described by an effective model akin to uniaxial ferromagnets. For a consistent theoretical description both higher-order anisotropy contributions and dipolar stray-fields have to be taken into account near the spin-flop. In particular, thermodynamically stable multidomain states exist in the spin-flop region, owing to the phase coexistence at this first-order transition. For this region, equilibrium spin-configurations and parameters of the multidomain states are derived as functions of the external magnetic field. The components of the magnetic susceptibility tensor are calculated for homogeneous and multidomain states in the vicinity of the spin-flop. The remarkable anomalies in these measurable quantities provide an efficient method to investigate magnetic states and to determine materials parameters in bulk and confined antiferromagnets, as well as in nanoscale synthetic antiferromagnets. The method is demonstrated for experimental data on the magnetic properties near the spin-flop region in the orthorhombic layered antiferromagnet $(C_2H_5NH_3)_2CuCl_4$.

PACS numbers: 75.50.Ee, 75.30.Kz, 75.60.Ch, 75.30.Cr

I. INTRODUCTION

In antiferromagnetic crystals with a preferable direction of the magnetization, a sufficiently strong magnetic field applied along this *easy axis* direction "overturns" the sublattice magnetization vectors $\mathbf{M}_1$ and $\mathbf{M}_2$ (Fig. 1). Néel demonstrated this threshold-field effect theoretically for classical two-sublattice antiferromagnets with sufficiently weak anisotropy in 1936.[1] Fifteen years later, this prediction of a jump-like reorientation transition driven by an external magnetic field was confirmed by experiments on the antiferromagnet $CuCl_2{\cdot}2H_2O$.[2] Since that time the *spin-flop* transition[3] has been observed and was investigated in great detail for a large group of antiferromagnets (see, e.g., Refs. [4,5,6,7,8] and further examples and bibliography in Refs. [9,10,11]). Originally, the name spin-flop (SF) transition was restricted to the field-driven reorientation transition in two-sublattice collinear easy-axis antiferromagnets following Néel's prediction. However, in many other classes of antiferromagnets similar mechanisms cause different types of field-driven reorientation effects so that one can speak about a class of spin-flop phenomena in a wider sense. These include field-driven transitions in antiferromagnets with a Dzyaloshinskii-Moriya interaction,[8,12] in multisublattice,[13,14] and in noncentrosymmetric antiferromagnets.[11]

The spin-flop transition comprises in a simple form main features of magnetic reorientation and phase transitions and it gives rise to various remarkable physical anomalies. It was found that the spin-flop transition is very sensitive to direction and values of the applied field[15,16] and specific transitional domain structures are formed in the spin-flop region.[10,17] These effects have been observed in MnF_2[18] and some other antiferromagnets.[19,20] Theory also predicts a specific reconstruction of the domain walls in the vicinity of the spin-flop[10,21] and extraordinary surface effects, which have been called "surface spin-flop".[22] The investigations on spin-flops made important contributions not only to different research topics in magnetism, but also to such general fields of physics as thermodynamics,[10,23] nonlinear physics,[24,25] and the theory of phase transitions and critical phenomena.[26]

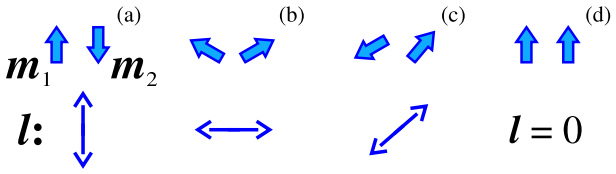

FIG. 1: Basic spin-configurations in collinear uniaxial antiferromagnets. At zero field the magnetization vectors $\mathbf{m}_i$ are antiparallel (a). The magnetic fields along the easy direction $H > H_0$ stabilizes the *spin-flop* phase (b). In magnetic fields deviating from the easy direction *canted* states are realized (c). In a sufficiently strong magnetic fields, $H > H_e$, the spin-flop and canted states transform into the saturated *flip* phase (d). These solutions are degenerate with respect to the sign of the staggered vector $\mathbf{l}$, which is represented by two-headed arrows in the bottom panel.

During the last decade spin-flops have been identified and studied in many novel bulk antiferro-

magnets including such classes as antiferromagnetic semiconductors,[27] organic magnets,[28] in cuprates, such as La_2CuO_4 and Nd_2CuO_4, being base materials for high-temperature superconductors,[13], or in noncentrosymmetric antiferromagnets.[11,29] However, the focus of current interest in spin-flops has now shifted towards nanomagnetic systems. Many of recently synthesized nanostructured materials have magnetic constituents with antiferromagnetic coupling. This vast and intensively investigated class of *antiferromagnetic* nanostructures includes different types of ferromagnetic/antiferromagnetic bilayers.[30] *Synthetic* or *artificial* antiferromagnets are recently designed for high-density storage technologies, spin-valves and magnetic random access memory (MRAM) devices.[31,32] In addition to layered systems nanoparticles of antiferromagnetic materials are currently investigated.[33] A variety of *size-dependent* electronic and magnetic effects are intensively investigated in many of these nanostructures.[34,35] In particular, experiments indicate that in ferro/antiferromagnetic bilayers the reorientation within the antiferromagnetic structures strongly influences the interface interactions and thus magnetic properties of the ferromagnetic subsystem.[36,37] A rich variety of specific field-induced reorientational effects have been found in synthetic antiferromagnets such as toggle mode MRAM devices,[38,39] and finite antiferromagnetic superlattices.[35,40]

In a broader context, new methods for the investigations of antiferromagnets in the bulk or close to antiferromagnetic surfaces,[24,41,42] and of nanostructured antiferromagnets[33,35,36,37,41] provide a wealth of data on spin-reorientation effects. These investigations require a refined theoretical description of these phenomena. The theoretical understanding of the the spin-flop was developed during many years of investigations with contributions from many researchers and great progress towards an understanding of the magnetic states near the spin-flop transitions has been reached. Still, the present stage of the theory is mostly dedicated to separate phenomena and a coherent description of the magnetization processes near spin-flops was not presented yet. This problem is evidently one that should be addressed with phenomenological approaches of magnetism, i.e., a "micromagnetism" for antiferromagnetics.[43] First solutions were obtained for fields applied along the easy axis[44,45]. The stability limits forming "critical astroids" in oblique magnetic fields, i.e. in fields deviating from the easy-axis, and the "critical angle of the spin-flop" were calculated in Refs. [15] for a model with second-order anistropy. The influence of the fourth-order anisotropy on the metastable states has been investigated in Ref. [46]. In Ref. [16] the problem has been reduced to an effective model akin to the usual reorientation in a uniaxial ferromagnet, and a complete set of solutions was derived.

In this paper we give a comprehensive phenomenological theory of the magnetic states and their evolution in applied fields for a two-sublattice collinear antiferromagnet. The model is explained in section II. We calculate all possible magnetic configurations in the system (section III) and give a physically clear description of the main features of the magnetization processes. In particular we calculate and analyse the tensor of the static magnetic susceptibility (sections III B and IV). This enable us to generalize and systematize results on bulk spin-flop and formulate directions for the investigation of this transition in bulk antiferromagnets and in antiferromagnetic nanostructures. In section IV the occurrence of multidomain states by demagnetization effects is analysed. There are characteristic peculiarities of the field and angular dependencies of the magnetic susceptibility, which can be employed in experiments on the spin-flop transition. In section V we demonstrate this approach based on experimental data for orthorhombic $(C_2H_5NH_3)_2CuCl_4$, which is a layered model antiferromagnet.[47]

II. MODEL AND EQUATIONS

Within the phenomenological theory of magnetism the magnetic (free) energy for a bulk *collinear* two-sublattices antiferromagnet can be written in the following form[10,44]

$$\begin{aligned} W &= \int w(\mathbf{m}_1,\mathbf{m}_2)dV \qquad (1)\\ &= \int \Big\{ J\mathbf{m}_1\cdot\mathbf{m}_2 + e_a(\mathbf{m}_1,\mathbf{m}_2) \\ &\quad -\mathbf{H}^{(\mathrm{e})}\cdot(\mathbf{m}_1+\mathbf{m}_2)M_0^{-1} \\ &\quad -\frac{1}{2}\mathbf{H}^{(\mathrm{m})}\cdot(\mathbf{m}_1+\mathbf{m}_2)M_0^{-1}\Big\}M_0^2\,dV. \end{aligned}$$

We assume here that the vectors of the sublattice magnetizations $\mathbf{M}_j$ do not change their modulus and their orientations are described by unity vectors $\mathbf{m}_j = \mathbf{M}_j/M_0$, $M_0 = |\mathbf{M}_j|$. Hence, we develop our theory for constant low temperatures in the antiferromagnetically ordered state. The energy (1) consists of the exchange interaction with exchange constant$J$, the magnetocrystalline anisotropy energy e_a, and Zeeman energy contributions due to the external magnetic field $\mathbf{H}^{(\mathrm{e})}$ and the demagnetization field $\mathbf{H}^{(\mathrm{m})}$, the latter giving the dipolar stray field energy. In this paper we are interested in antiferromagnets with a preferable direction of a magnetic ordering, i.e. *easy-axis* systems. In uniaxial antiferromagnets the *easy-axis* coincides with the principal axis of symmetry, and in orthorhombic crystals with one of the orthorhombic axis. In this paper we chose coordinates such that the easy axis is along the z-axis. The energy density $e_a = e_a^{(u)} + e_a^{(b)}$ includes uniaxial $e_a^{(u)}$ and in-plane $e_a^{(b)}$ parts. The uniaxial anisotropy $e_a^{(u)}$ consists of invariants of type $m_{1z}^{2(n-k)}m_{2z}^{2k}$ where n is an integer, and $k = 1, 2..n$.[44] These energy contributions strongly decrease with increasing n. In the vicinity of the spin-flop field the second-order uniaxial anisotropy is "can-

celled" by the applied magnetic field. Hence, higher-order terms must be be taken into account.[10,16] Therefore, both second-order and fourth-order terms must be included in the theory for spin-flops. One can write the uniaxial anisotropy as[10]

$$\begin{aligned} e_a^{(u)}(m_{1z}, m_{2z}) \;=\; & -\frac{K}{2}(m_{1z}^2 + m_{2z}^2) - K' m_{1z} m_{2z} \\ & -\frac{K_{20}}{4}(m_{1a}^4 + m_{2a}^4) \\ & -\frac{K_{21}}{4} m_{1a} m_{2z}(m_{1a}^2 + m_{2a}^2) \\ & -\frac{K_{22}}{2} m_{1a}^2 m_{2a}^2 \,. \end{aligned} \tag{2}$$

Usually, the second-order terms with constants K, K' play the dominant role for the orientation of the magnetic vectors. But, the fourth-order terms with $n = 2$ and constants K_{2k} become vital near the spin-flop, as will be shown later.

The anisotropy energy in the basal plane $e_a^{(b)}$ includes invariants composed of in-plane components of the vectors $\mathbf{m}_i$ and, depending on the crystal symmetry, includes quadratic terms for orthorhombic crystals or terms of higher degree for uniaxial crystals. These energy contributions lead to additional orientational effects. They determine one preferable direction for orthorhombic symmetry or more directions for uniaxial antiferromagnets for the spin orientation in the basal plane perpendicular to the magnetic easy axis.

The model Eq. (1) with anisotropy (2) describes a vast group of antiferromagnetic crystals with collinear order, including such well-studied compounds as MnF_2, FeF_2, Cr_2O_3, $GdAlO_3$ and others.[10] In this class of antiferromagnets effects of magnetic couplings are absent that violate a *collinear* and spatially homogeneous order in the ground state, such as competing exchange or Dzyaloshinkii-Moriya interactions.[11]

The equations minimizing the energy functional (1) together with the Maxwell equations for the magnetostatic problem determine the distributions of the magnetization fields $\mathbf{m}_i(\mathbf{r})$ and the stray field $\mathbf{H}^{(\mathrm{m})}(\mathbf{r})$ in the sample.[43] These integro-differential equations are too complex and impractical, even for brute-force numerical calculations. However, the problem can be reduced to a number of simplified auxiliary problems.[10,43] Following these standard methods we start from the analysis of spatially homogeneous states in *fixed* internal magnetic fields $\mathbf{H} = \mathbf{H}^{(\mathrm{e})} + \mathbf{H}^{(\mathrm{m})}$.

In the antiferromagnetic crystals displaying a spin-flop, the exchange coupling is much stronger than the anisotropy energy, $J \gg w_a$. In this case it is convenient to use the *net magnetization* vector, $\mathbf{m} = (\mathbf{m}_1 + \mathbf{m}_2)/2$, and the *staggered magnetization* vector (or vector of antiferromagnetic order), $\mathbf{l} = (\mathbf{m}_1 - \mathbf{m}_2)/2$, as internal variables of the system. Because $|\mathbf{m}_i| = 1$ these vectors satisfy the constraints $\mathbf{m} \cdot \mathbf{l} = 0$, $\mathbf{m}^2 + \mathbf{l}^2 = 1$.[44] Independent minimization of (1) with respect to $\mathbf{m}$ yields (see Refs. [11,12] for details)

$$\mathbf{m} = [\mathbf{H} - \mathbf{n}(\mathbf{H} \cdot \mathbf{n})]/H_{\mathrm{e}}, \qquad H_{\mathrm{e}} = (2JM_0)\,, \tag{3}$$

where $\mathbf{n} = \mathbf{l}/|\mathbf{l}|$ is the unity vector along the staggered magnetization and H_{e} is the so-called exchange field. As follows from (3), in this field $\mathbf{m} = 1$, i.e. the magnetization vectors align along the field direction, which is a *spin-flip* transition. After substitution of (3) and omitting gradients of $\mathbf{m}$ the energy density w in Eq. (1) can be written as a function of the vector $\mathbf{n}$ alone

$$w = -\frac{1}{2J}[\mathbf{H}^2 - (\mathbf{H} \cdot \mathbf{n})^2] + e_a(\mathbf{n}) M_0^2 \,. \tag{4}$$

For the collinear antiferromagnets, further simplifications are possible by restricting the spatial orientation of the magnetization vectors. In most practically important cases, the equilibrium configurations $\mathbf{m}_i$ and, correspondingly, the vectors $\mathbf{m}$ and $\mathbf{l}$ remain in or close to the plane spanned by the easy axis and the magnetic field.[16] In this paper, we chose coordinates with $x0z$ as this plane. The restriction on the magnetic configurations always holds true when the vector $\mathbf{H}$ remains in the plane spanned by the "easy" and the "intermediate" axes of an orthorhombic antiferromagnet. In the uniaxial antiferromagnets, in-plane components of the magnetic field usually suppress orientational effects of the weak in-plane anisotropy $w_a^{(b)}$. Then, the vectors $\mathbf{m}_i$ of equilibrium states remain in the $x0z$ plane. This means that only the uniaxial anisotropy (2) may essentially influence the magnetic states. For the magnetic energy in terms of $\mathbf{m}$ and $\mathbf{l}$, a systematic analysis (see Ref. [16]) shows that only the following terms from the uniaxial anisotropy (2) must be retained,

$$e_a^{(u)} = -(K + K')m_z^2 - B_1 l_z^2 - B_2 l_z^4, \tag{5}$$

where $B_1 = K - K'$, $B_2 = (K_{20} - K_{21} + K_{22})/2$. Then, within the $x0z$ plane the magnetic states are described by only one internal variable, the angle θ between the easy axis and the staggered magnetization. The expansion of the energy in terms of θ with respect to the small parameter $|e_a^{(u)}|/J$ yields the leading contribution

$$w_0^{(1)}(\theta) = (4J)^{-1} \left[\left(H_z^2 - H_x^2 - H_0^2\right)\cos 2\theta + 2H_x H_z \sin 2\theta\right], \tag{6}$$

$$H_0 \;=\; \sqrt{2JB_1}M_0, \tag{7}$$

and the contributions to next order

$$\begin{aligned} w_0^{(2)}(\theta) \;=\; & -\frac{H_0^2}{4J}\left(\frac{B_2}{2B_1} + \frac{K}{2J}\right)\cos^2 2\theta \\ & -\frac{H_0^2}{4J}\left(\frac{B_2}{2B_1} + \frac{K - K'}{2J}\right)\cos 2\theta \,. \end{aligned} \tag{8}$$

In the transformation of the energy density (4) into the simplified energy density $w_0(\theta) = w_0^{(1)}(\theta) + w_0^{(2)}(\theta)$ with

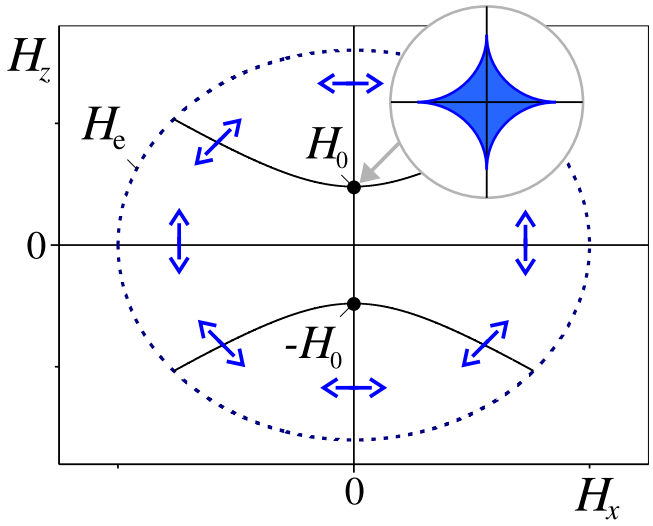

FIG. 2: (H_x, H_z) phase diagram for easy-axis antiferromagnets. The *dashed* line H_e gives the continuous transition into the saturated states. The shaded area is the region of the metastable states in the vicinity of the critical field $(H_x = 0, H_z = H_0)$. Details of the phases diagram in these regions are shown in the next figure.

the contributions from Eqs. (6) and (8), we have omitted higher-order terms and a constant combination of materials constants. The coefficients in $w_0^{(1)}$ in Eq. (6) are proportional to H^2. They are generally much larger than those in $w_0^{(2)}$. In wide regions of the magnetic phase-diagram $w_0^{(1)} \gg w_0^{(2)}$ and the energy contribution $w_0^{(2)}$ can be neglected. However, as the magnetic field approaches the critical point (H_x, H_z)=$(0, H_0)$ the leading energy term in (6) vanishes and the term $w_0^{(2)}$ from Eq. (8) must be taken into account. In next sections we analyze the magnetic states for model (6), (8).

III. MAGNETIC PHASE DIAGRAMS

A. Equilibrium magnetic configurations

Outside the spin-flop region the equilibrium states are described by the energy $w_0^{(1)}(\theta)$ (6). In easy-axis antiferromagnets the staggered vector $\mathbf{l}$ interacts with the applied magnetic field via the coupling to the magnetization vector $\mathbf{m} \perp \mathbf{l}$ according to Eq. (3). Correspondingly the interaction with the applied field favours the state $\mathbf{l} \perp \mathbf{H}$. Note that in isotropic systems one has $H_0 = 0$, and the energy density $w_0^{(1)}(\theta) = H^2 \cos(2\theta - 2\psi)$ with ψ the angle between $\mathbf{H}$ and z-axis has minima for $\theta = \psi \pm \pi/2$. In easy-axis antiferromagnets the uniaxial anisotropy orientates $\mathbf{l}$ along the easy axis. The competition between these two magnetic couplings determines the equilibrium states. These states are sketched in the (H_x, H_z) phase diagram, Fig. 2. Minimization of (6) leads to the well-known *Néel formula*[1] for the magnetic configurations,

$$\tan 2\theta = \frac{2H_z H_x}{H_z^2 - H_x^2 - H_0^2}\,. \qquad (9)$$

Because the energy is invariant under the transformation $\theta \to \theta + \pi$, Eq. (9) describes solutions with antiparallel directions of the staggered vector. The equilibrium states $\theta_{1,2}$ correspond to the minima of the leading energy Eq. (6), which are given by $w_0^{(1)}(\theta_1) = w_0^{(1)}(\theta_2) \equiv \min[w_0^{(1)}(\theta)]$. These wells in the potential energy Eq. (6) are separated by a barrier. The *height* of this potential barrier is $\Delta w = \max[w(\theta)] - \min[w(\theta)]$. For the potential (6) we obtain

$$\Delta w_0^{(1)} = \frac{1}{2J}\sqrt{\left(H_z^2 - H_x^2 - H_0^2\right)^2 + 4H_x^2 H_z^2}\,. \qquad (10)$$

In a magnetic field directed along the easy axis $H_x = 0$ the *collinear* antiferromagnetic phase for $H < H_0$ and the *spin-flop* phase in the field range $H_0 < H < H_e$ correspond to the two branches of solutions for Eq. (9) with $\theta = 0$ and $\theta = \pi/2$, respectively (Fig. 1(a),(b)). In magnetic fields that deviate from the easy axis, *angular* or *canted* phases are realized (Fig. 1(c)). The equilibrium states described by Eq. (9) result from the competition between the uniaxial anisotropy, which favours the orientation of the staggered magnetization $\mathbf{l}$ along the easy axis and the magnetic field, which orientates $\mathbf{l}$ perpendicular to its direction. At low fields the net magnetization is very small $|\mathbf{m}| \ll |\mathbf{l}|$, so the energy contribution $B_1 l_z^2$ plays the dominating role for the orientation of the magnetic configuration. The characteristic field H_0 given by a geometrical mean of the intra-sublattice exchange J and the second-order anisotropy for the staggered vector B_1 measures the scale of the energy contributions favouring the easy-axis ground state. Thus, for small fields $|\mathbf{H}| < H_0$ the anisotropy prevails and stabilizes states with the staggered vector $\mathbf{l}$ nearly parallel to the easy-axis, $\theta \ll 1$, with small magnetization, $m \ll 1$.

In an increasing field $\mathbf{l}$ rotates towards the direction perpendicular to $\mathbf{H}$, and the net magnetization m gradually increases. In the (H_x, H_z) phase diagram (Fig. 2) the hyperbola, $H_z^2 - H_x^2 = H_0^2$, separates the regions with the angles $|\theta|$ larger and smaller $\pi/4$. At $H = H_e$ the antiferromagnet transforms into the saturated state with $m = 1$ along the applied field, $\mathbf{m} || \mathbf{H}$.

The Néel equation Eq. (9) has a singularity at $(H_x, H_z) = (0, H_0)$. At this point $(0, H_0)$ in the phase-diagram the main competing forces completely compensate each other: the leading energy contribution (6) equals zero, and the next order energy contribution $w_0^{(2)}$ in Eq. (8) plays a decisive role. In this region, the full energy of the model $w^{(0)}(\theta))$ can be written as

$$\begin{aligned} w_0(\theta) \;&=\; -\frac{\varkappa}{4J} H_0^2 \cos^2 2\theta \qquad (11) \\ &+\; \frac{1}{4J}\left[\left(H_z^2 - H_x^2 - H_{\rm SF}^2\right)\cos 2\theta \; + 2H_x H_z \sin 2\theta\right] \end{aligned}$$

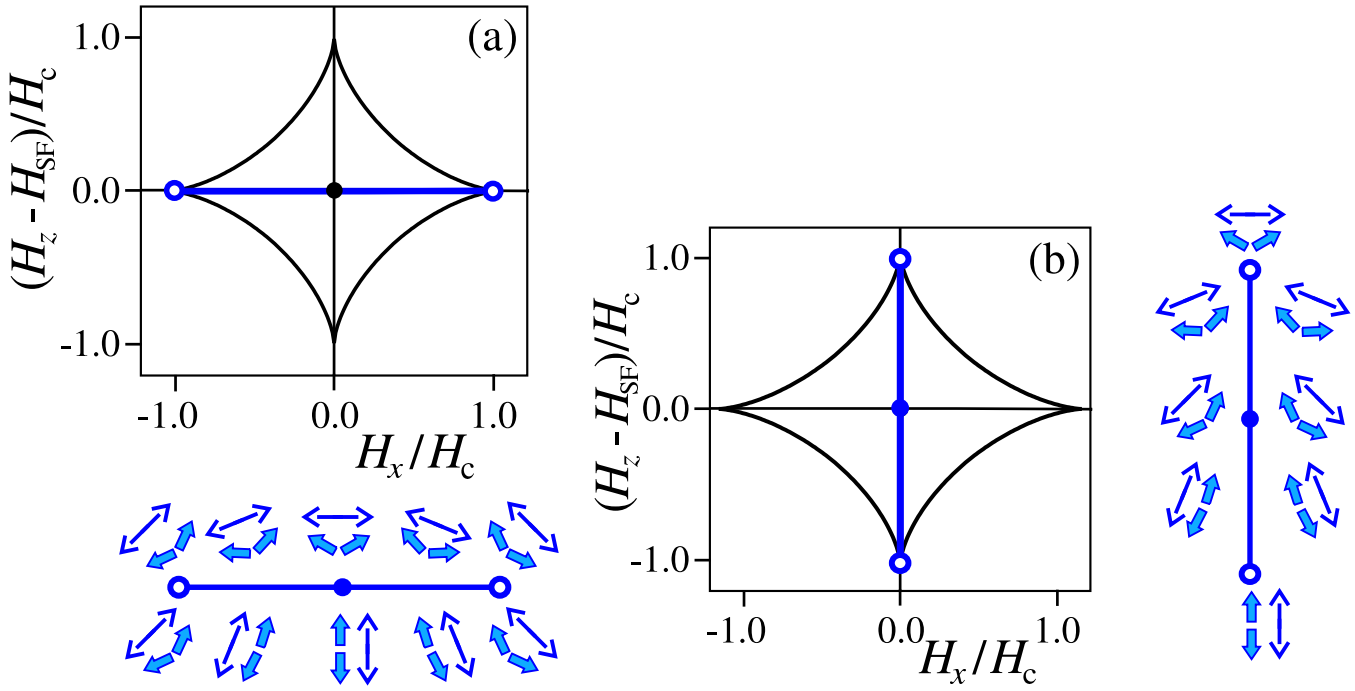

FIG. 3: Details of the phase diagram Fig. 2 in the vicinity of the spin-flop field depend on the sign of $\varkappa$ as defined in Eq. (11): (a) $\varkappa > 0$, (b) $\varkappa < 0$. Thin lines confine the astroid regions with metastable states. Thick line segments give the first-order transition lines. The arrows show spin-configurations in the competing phases along the transition. Hollow points are the end points of the first-order transitions.

with

$$\varkappa = \frac{B_2}{2B_1} + \frac{K}{2J}, \tag{12}$$

$$H_{\rm SF} = H_0 + \Delta H_0, \tag{13}$$

$$\Delta H_0 = \sqrt{2JB_1}M_0\left(\frac{K+K'}{4J} + \frac{B_2}{2B_1}\right). \tag{14}$$

Eq. (11) represents a consistent expression for the phenomenological energy near the SF field $(0, H_0)$. It includes those higher-order interaction terms that are mandatory owing to the compensation of leading energy contributions (see Eq. (6)). These additional terms consist of inter- and intra-sublattice uniaxial second-order anisotropy terms with parameters K, K' and the fourth-order anistropy B_2 of the staggered vector. Comparing energy densities $w_0^{(1)}$ from Eq. (6) with Eq. (11) we find that these magnetic coupling terms (i) shift the value of the SF field $H_0 \to H_{\rm SF} = H_0 + \Delta H_0$, where $\Delta H_0 \ll H_0$, and (ii) create an additional interaction term proportional to $\cos^2 2\theta$. This energy contribution stabilizes the magnetic states at the SF field $(0, H_{\rm SF})$ because it provides a potential barrier $\Delta w_0(H_{\rm SF}) = |\varkappa| H_0^2/(2J)$.

Due to the relations $|K|, |K'|, |K_{2k}\| \ll J$, $|B_2| \ll |B_1|$ the region, where $w_0^{(1)}$ and $w_0^{(2)}$ have the same order, is restricted to the close vicinity of the point $(H_x = 0, H_z = H_0)$: $|H_z - H_0| \ll H_0, |H_x| \ll H_0$. In this region the energy density $w_0(\theta) = w_0^{(1)}(\theta) + w_0^{(2)}(\theta)$ can be reduced to the potential expression

$$\Phi(\theta) = \frac{2Jw_0}{H_0} = -\frac{\mathrm{sign}(\varkappa)}{2} H_{\rm c} \cos^2 2\theta + (H_z - H_{\rm SF}) \cos 2\theta + H_x \sin 2\theta\,. \tag{15}$$

Here, the characteristic field

$$H_{\rm c} = |\varkappa| H_0 = \left|\frac{B_2}{2B_1} + \frac{K}{2J}\right| \sqrt{2JB_1} M_0 \ll H_0 \tag{16}$$

sets the scale of the field region around the critical field $(0,H_0)$, where the interactions described by the energy density (15) produce noticeable effects. The energy density $\Phi(\theta)$ (15) functionally coincides with that of a uniaxial ferromagnet

$$\Phi_f(\phi) = -\frac{1}{2}\beta M_0 \cos^2\phi - H_z \cos\phi - H_x \sin\phi\,, \tag{17}$$

where β is the anisotropy constant, ϕ is the angle between the magnetization $\mathbf{M}$ and the $0z$ axis.[43] In the ferromagnetic model (17) the anisotropy field $H_a = |\beta| M_0$ corresponds to the characteristic field $H_{\rm c}$ in (15), the components of the magnetic field (H_x, H_z) correspond to $(-H_x, -(H_z - H_{\rm SF})$, and the angle ϕ to the angle 2θ. Thus, the behaviour of the uniaxial antiferromagnet is reduced to the well-known model and the corresponding mathematical results for the magnetic states of uniaxial ferromagnets.[43,48]

For the model (15) the equation for the equilibrium state $d\Phi/d\theta = 0$ is

$$\begin{aligned} &\mathrm{sign}(\varkappa) H_{\mathrm{c}} \sin 2\theta \cos 2\theta \\ &-(H_z - H_{\mathrm{SF}}) \sin 2\theta \ + \ H_x \cos 2\theta = 0 \end{aligned} \tag{18}$$

and the existence region for metastable states is bounded by the astroid

$$H_x^{2/3} + (H_z - H_{\mathrm{SF}})^{2/3} = H_{\mathrm{c}}^{2/3} \, . \tag{19}$$

The polar angle for the cusps on the sides of the astroid

$$\psi_{\mathrm{c}} = \arctan(|H_{\mathrm{c}}|/H_0) = \arctan(\varkappa) \approx \varkappa, \tag{20}$$

is the so-called *critical angle of the spin-flop*. This is the maximal angle for the existence of the metastable states in obliquely applied magnetic fields. The notion of this "critical angle" was introduced in Ref. [15], where the astroids of type (19) have been calculated for the model with second-order anisotropy. The character of the magnetic states within the astroid (19) depends on the sign of the parameter $\varkappa$ (11):
(i) For $\varkappa > 0$ in magnetic field $H_z = H_{\mathrm{SF}}$, $H_x = 0$, the first-order transition occurs between the antiferromagnetic and spin-flop phase. This is the proper jump-like *spin-flop transition*. Note that the characteristic field H_0 in the Néel equation (9) differs from the spin-flop field H_{SF}, Eq. (14). At finite transversal components of the magnetic field H_x the first-order transition happens between distorted AF and SF, i.e., canted phases at the line $(H_z = H_0, |H_x| \leq \varkappa)$ (Fig. 3(a)). The solutions for these competing phases are (cf. Ref.[16])

$$\theta_1 = -\frac{1}{2} \arcsin(H_x/H_{\mathrm{c}}), \quad \theta_2 = -\pi/2 - \theta_1 \, . \tag{21}$$

For increasing $H_x < H_{\mathrm{c}}$ the difference between the competing canted phases decreases. This difference disappears at endpoints of the first-order transition lines. These endpoints are located at the cusps of the astroid (19), $(H_{\mathrm{c}}, H_{\mathrm{SF}})$, $(-H_{\mathrm{c}}, H_{\mathrm{SF}})$. The configuration of the magnetic states in these points is for both phases $\theta_{1,2} = \mp\pi/4$ (Fig. 3(a)).
(ii) For $\varkappa < 0$, the canted phases exist as stable states even in magnetic fields along the easy axis within the astroid (19). Minimization of (11) for this case yields the deviation angle of the solutions from the easy-axis

$$\theta_b = \pi - \arccos[(H_z - H_0)/|H_{\mathrm{c}}|] \, . \tag{22}$$

These solutions describe a continuous rotation of the staggered vector $\mathbf{l}$ from the AF phase at the low cusp, $H_z = H_0 - |H_{\mathrm{c}}|$, to the SF phase at the high cusp, $H_z = H_0 + |H_{\mathrm{c}}|$ (Fig. 3(b)). The plane(s) of this rotation are determined by in-plane magnetic anisotropy. Depending on the crystal symmetry there are several such planes (half-planes) spanned by the easy-axis and easy magnetization directions in the basal plane. This degeneracy of the magnetic states is lifted by a deviation of the applied field from the easy axis. In such a field, the canted state with the largest projection of $\mathbf{m}$ onto the field direction corresponds to the stable states, while other states preserve metastability for small deviations of the field and become unstable for larger deviations. This means that the vertical axis of the astroid (19) given by $H_0 - |H_{\mathrm{c}}| < H_z < H_0 + |H_{\mathrm{c}}|$ is a first-order transition line between several canted phases. In particular, in orthorhombic antiferromagnets there is only one plane of rotation (spanned by the easy and intermediate axis) and the phase transition occurs between two canted phases with opposite rotation sense. Such magnetic states have been studied in Ref. [16].

In next subsections we analyze field dependencies of the magnetization and the magnetic susceptibility.

B. Magnetization and magnetic susceptibility

For the field dependencies of the net magnetization $\mathbf{M} = M_0(\mathbf{m}_1 + \mathbf{m}_2) = 2M_0\mathbf{m}$, one derives from (3)

$$\begin{aligned} M_x &= \frac{M_0}{2J} \left[H_x(1 + \cos 2\theta) - H_z \sin 2\theta \right] \\ M_z &= \frac{M_0}{2J} \left[H_z(1 - \cos 2\theta) - H_x \sin 2\theta \right] \, , \end{aligned} \tag{23}$$

where θ is the solutions of the equations (9) and (18) minimizing the energy. For the calculation of the magnetization vector and susceptibility tensor in the vicinity of the SF field, it is convenient to rewrite the components of the total magnetization (23) in the following form

$$\begin{aligned} M_x &= M_{\mathrm{SF}} \left[-\sin 2\theta + \mu_1(\theta) \right] , \\ M_z &= M_{\mathrm{SF}} \left[(1 - \cos 2\theta) + \mu_2(\theta) \right] \, , \end{aligned} \tag{24}$$

where

$$\begin{aligned} \mu_1(\theta) &= \frac{|\varkappa|}{H_{\mathrm{c}}} \left[H_z \sin 2\theta + H_x(1 + \cos 2\theta) \right] , \\ \mu_2(\theta) &= \frac{|\varkappa|}{H_{\mathrm{c}}} \left[H_z(1 - \cos 2\theta) - H_x \sin 2\theta \right] \, . \end{aligned} \tag{25}$$

The magnetization

$$M_{\mathrm{SF}} = M_0 \sqrt{\frac{B_1}{2J}} = M_0 \left(\frac{H_0}{H_{\mathrm{e}}} \right) \tag{26}$$

characterizes the typical values of the net magnetization in the spin-flop region. By virtue of the relation $H_{\mathrm{e}} \gg H_0$ the magnetization M_{SF} amounts only to a small fraction of the saturation value M_0.

In the SF region, given by $H_x, H_z \lesssim H_{\mathrm{c}}$, see Eq. (15), the functions μ_1 and μ_2 are very small, $\mu_i \ll 1, i = 1, 2$, and can be omitted. By substituting the solutions (21) into (23) we obtain the magnetization on the transition

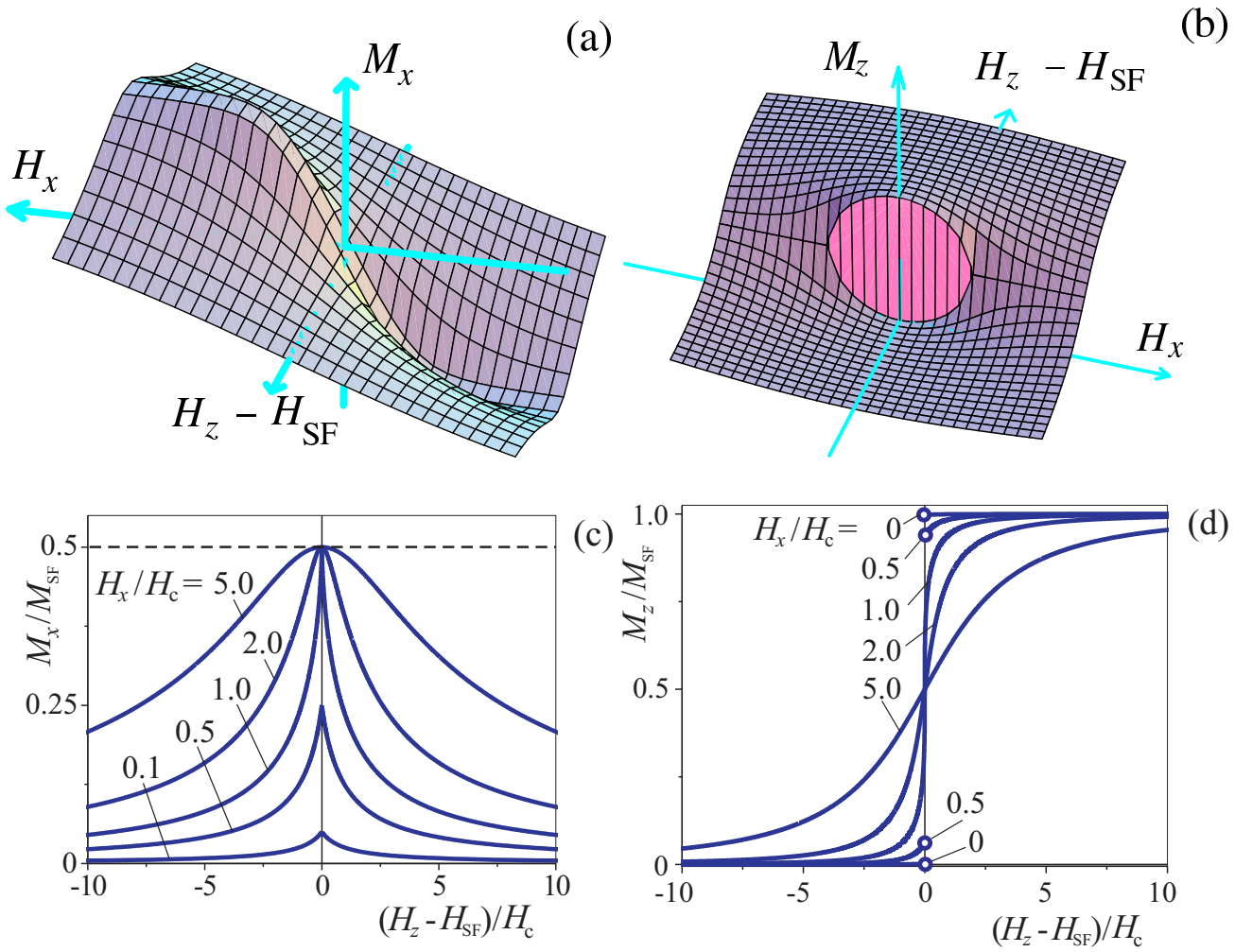

FIG. 4: Field dependencies of the magnetization components near the SF field for $\varkappa > 0$: transverse $M_x(H_x, H_z)$(a), longitudinal $M_z(H_x, H_z)$ (b) and their projections onto the $(H_z, M_{x(z)})$ planes (c), (d). Only the magnetization curves corresponding to the stable states are plotted.

line for $\varkappa > 0$,

$$M_x^{(1)} = M_x^{(2)} = \frac{M_{SF}}{2}\left(\frac{H_x}{H_c}\right),$$
$$M_z^{(1,2)} = \frac{M_{SF}}{2}\left[1 \mp \sqrt{1-\left(\frac{H_x}{H_c}\right)^2}\right]. \qquad (27)$$

The transverse components M_x are equal in both phases. The longitudinal components undergo a jump $\Delta M_z = M_{SF}\sqrt{1-(H_x/H_c)^2}$ at the SF (Fig. 4). The parameter M_{SF} Eq. (26) is equal to the maximum value of the magnetization jump at the SF transition.

For $\varkappa < 0$ the magnetization in the competing phases have antiparallel components perpendicular to the easy axis, while the parallel components are equal

$$M_x^{(1,2)} = \mp\frac{M_{SF}}{2}\sqrt{1-\left(\frac{H_z - H_{SF}}{H_c}\right)^2},$$
$$M_z^{(1)} = M_z^{(2)} = \frac{M_{SF}}{2}\left[1 + \left(\frac{H_z - H_{SF}}{H_c}\right)\right]. \qquad (28)$$

In this case the transverse components M_x undergo a jump given by $\Delta M_x = M_{SF}\sqrt{1-(H_z - H_{SF})^2/H_c^2}$ at the first-order transition.

The landscapes of the magnetization "surfaces" $M_x(H_x, H_z)$, $M_x(H_x, H_z)$ near the first-order transition and in the adjacent regions of the phase-space are shown in Fig. 4. The shape of these surfaces is reflected by peculiarites of the magnetic susceptibility. The components of the tensor of the *internal* static magnetic susceptibility,

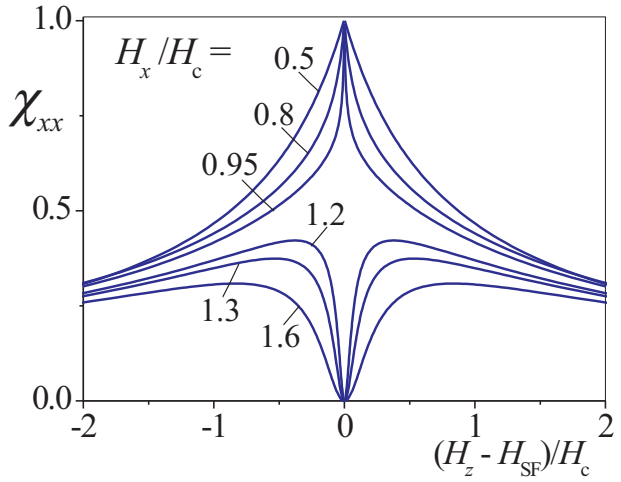

FIG. 5: Field dependencies of $\chi_{xx}(H_z)$ for various values of H_x. This and in two following figures display susceptibility components for antiferromagnets with $\varkappa > 0$. The susceptibility units are $1/(4J\varkappa)$. Only the branches corresponding to the stable states are plotted.

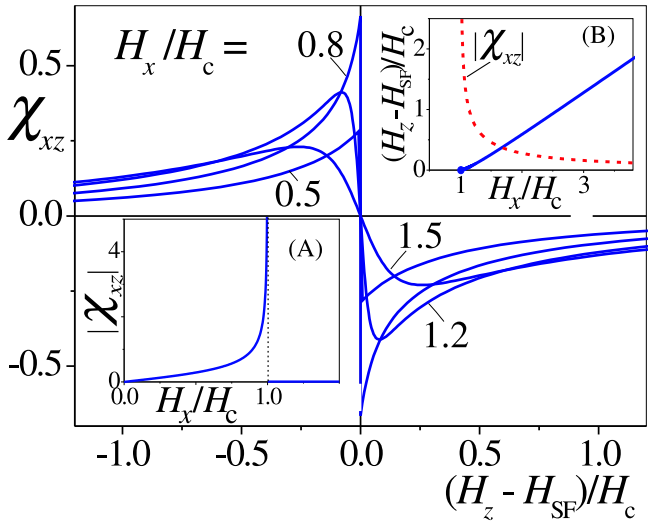

FIG. 6: Field dependencies of $\chi_{xz}(H_z)$. Inset (A) shows $\chi_{xz}(H_x)$ at the transition line $H_z = H_{SF}$. In Inset (B), the location of the extremal values from Eq. (35) are plotted by a solid line and their amplitudes from Eq. (36) by a dashed line.

$\chi^{(i)}_{ij} = \partial M_i/\partial H_j$, are derived from the equations (cf. [49])

$$\chi^{(i)}_{xx} = \frac{1}{4J}[1 + \cos 2\theta + 2H^2\Omega(\theta)\cos^2(2\theta - \psi)],$$
$$\chi^{(i)}_{xz} = \frac{1}{4J}[\sin 2\theta + H^2\Omega(\theta)\sin(2\theta - \psi)\cos(2\theta - \psi)]$$
$$\chi^{(i)}_{zz} = \frac{1}{4J}[1 - \cos 2\theta + 2H^2\Omega(\theta)\sin^2(2\theta - \psi)], \quad (29)$$

where $\Omega^{-1}(\theta) = d^2\Phi(\cos 2\theta)/d(\cos 2\theta)^2$, $\Phi(\cos 2\theta)$ is derived from Eq. (15). These relations, together with Eq. (18) yield field dependencies of the magnetization

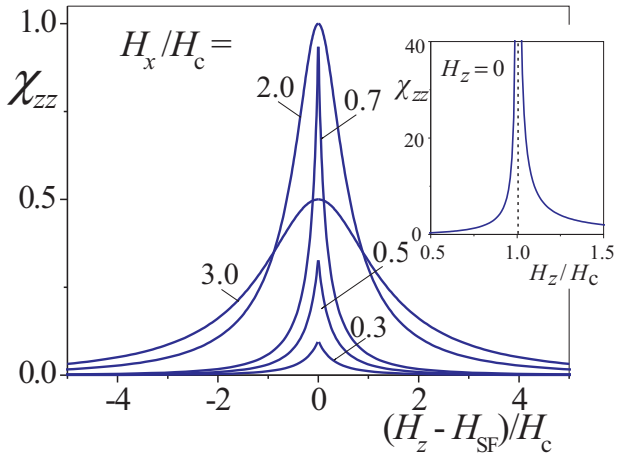

FIG. 7: Field dependencies of $\chi_{zz}(H_z)$ for various values H_x. The arrow-like shape of the functions $\chi_{xx}(H_z)$ within the transition region ($|H_x| < H_c$) changes into a bell-like shape outside this region. In both cases the functions $\chi_{zz}(H_z)$ have a maximum at $H_z = H_{SF}$. These maximum values are plotted as function of H_x in the inset.

components and the susceptibility tensor in the spin-flop region. Near the SF field the expansion of (29) with respect to the small parameter $\varkappa \ll 1$ allows a considerable simplification of the expressions for χ_{ij},

$$\chi_{xx} = -\frac{1}{4J|\varkappa|}\frac{\sin 2\theta \cos^2 2\theta}{(\mathrm{sign}(\varkappa)\sin^3 2\theta + H_x/H_c)}$$
$$= -\frac{1}{4J|\varkappa|}\frac{\cos^3 2\theta}{(\mathrm{sign}(\varkappa)\cos^3 2\theta - H_z/H_c)}, \quad (30)$$

$$\chi_{xz} = \frac{1}{4J|\varkappa|}\frac{\sin^2 2\theta \cos 2\theta}{(\mathrm{sign}(\varkappa)\sin^3 2\theta + H_x/H_c)}$$
$$= -\frac{1}{4J|\varkappa|}\frac{\sin 2\theta \cos^2 2\theta}{(\mathrm{sign}(\varkappa)\cos^3 2\theta - H_z/H_c)}, \quad (31)$$

$$\chi_{zz} = -\frac{1}{4J|\varkappa|}\frac{\sin^3 2\theta}{(\mathrm{sign}(\varkappa)\sin^3 2\theta + H_x/H_c)}$$
$$= \frac{1}{4J|\varkappa|}\frac{\sin^2 2\theta \cos 2\theta}{(\mathrm{sign}(\varkappa)\cos^3 2\theta - H_z/H_c)}. \quad (32)$$

For antiferromagnets with $\varkappa > 0$ the expressions from Eqs. (30), (31), and (32) for $\hat{\chi}_{ij}$ in dependence on H_x are convenient for numerical calculations and those depending on H_z in the case $\varkappa < 0$. As the field approaches the stability limits, given by the lines $\Phi_{\theta\theta} \equiv \partial^2\Phi/\partial\theta^2 \to 0$, the functions $\chi_{ij} \propto 1/\Phi_{\theta\theta}$ diverge. For applications to real antiferromagnets it is important to distinguish the branches of the functions $\chi_{ij}(H_x, H_z)$ corresponding to the stable states. Typical field dependencies of the components of $\hat{\chi}_{ij}$ for the stable phases are plotted in Figs. 5, 6, and 7. The functions $\chi_{xx}(H_z)$ have *qualitatively* different field dependencies within and outside the region near

the first-order transitions. In the former case $|H_x| < H_c$, the curves $\chi_{xx}(H_z)$ have arrow-like shape with a maximum at the transition field $H_z = H_{SF}$. In the latter case $|H_x| > H_c$, the curves $\chi_{xx}(H_z)$ have a minimum in fields along a line prolongating the transition line and two symmetric maxima

$$\chi_{xx}^{(\max)} = \frac{1}{4J\varkappa}\left(1 - \frac{1}{3\cos^2\alpha}\right) \tag{33}$$

for fields lower and higher than the SF field H_{SF}. The location of these maxima in (H_x, H_z) for $H_x > H_c$ is determined parametrically by a set of equations

$$\begin{aligned} H_x^{(\max 1)} &= \frac{2H_c\cos^3\alpha}{3\cos^2\alpha - 1}, \\ H_z^{(\max 1)} &= \pm\frac{H_c\sin^3\alpha}{3\cos^2\alpha - 1} \end{aligned} \tag{34}$$

with $\alpha = -\pi/2 - 2\theta$. For χ_{xz} (Fig. 6) stationary points

$$|\chi_{xz}^{(\max)}| = \frac{1}{8J\varkappa}\frac{3\cos^2\alpha - 2}{3|\sin\alpha|\cos\alpha} \tag{35}$$

are situated on the lines

$$\begin{aligned} H_x^{(\max 2)} &= \frac{H_c\cos^3\alpha}{3\cos^2\alpha - 2}, \\ H_z^{(\max 2)} &= \pm\frac{2H_c\sin^3\alpha}{3\cos^2\alpha - 2}. \end{aligned} \tag{36}$$

Similarly, functions $\partial\chi_{ij}/\partial H_k(\mathbf{H})$ also show qualitatively different dependencies in different parts of the phase diagram and include extremal points. The field values for all these anomalies are determined by the material constants of the antiferromagnets. This connection between anomalous field-dependence of the susceptibility tensor in the SF region and materials paramters can provide a basis for experimental approaches to investigate the magnetic properties and materials parameters in antiferromagnets. Values of magnetic interactions, in particular higher-order contributions to the magnetic anisotropy, can be determined by measurements of the susceptibility tensor in the SF region and fitting of the χ_{ij} data to the theoretical expressions shown above. This will be demonstrated in section V.

Here, we compare characteristic values of the magnetic susceptibility for antiferromagnets in the major part of the magnetic field phase diagram and in the SF region. In the (H_x, H_z) phase diagram (Fig. 2) saturation is achieved at the exchange field $|H| = H_e$. Thus, the average susceptibility is $\langle\chi\rangle_{AFM} = M_0/H_e = 1/(2J)$. This is exactly the value of the susceptibility in the SF phase. The metastable region in the phase diagram near the SF field has a width $\Delta H = 2H_c = 2H_0\psi_c$, Eq. (19), while the magnetization changes by $\Delta M = M_0H_0/H_e$, Eqs. (27), (28). Thus, the average susceptibility in this region can be estimated to $\langle\chi\rangle_{SF} = M_0/(2|\varkappa|H_e) = 1/(4J\varkappa) \simeq 1/(4J\psi_c)$. This average equals the expressions from Eqs. (30), (31), and (32) up to some numerical factor. The magnetic susceptibility near the SF field is strongly enhanced compared to the average susceptibility in the major part of the phase diagram, $\langle\chi\rangle_{SF} = \langle\chi\rangle_{AFM}(H_0/(2H_c))$. This enhancement is given by the ratio $(H_0/(2H_c)) = 1/(2\psi_c)$ which usually amounts to a factor of several hundreds. Note that the absolute change of the magnetization $\Delta M = M_0H_0/H_e \ll M_0$ is tiny. However, due to the extremely narrow width of the metastable region near the SF field, the magnetic susceptibility becomes very strong in this region.

As was mentioned above, similar functional expressions describe the field dependence of the magnetization $\mathbf{M}^{(f)}$ for the model of a uniaxial ferromagnet (17) and for the antiferromagnet in the SF regions following the basic approach Eq. (24) with $\mu_i = 0$. In fact, one can derive

$$\mathbf{M}(\mathbf{H}/H_c) = \left(\frac{H_0}{2H_e}\right)\mathbf{M}^{(f)}(\mathbf{H}/H_a) + M_0\left(\frac{H_0}{2H_e}\right)\mathbf{a}. \tag{37}$$

The last term in (37) signifies a shift in direction of the easy axis **a**. A corresponding relation between the components of the magnetic susceptibility near the SF transition and those of the ferromagnetic susceptibility $\chi_{ij}^{(f)}$ is given by

$$\chi_{ij}(\mathbf{H}/H_c) = \left(\frac{H_a}{2H_e|\varkappa|}\right)\chi_{ij}^{(f)}(\mathbf{H}/H_a). \tag{38}$$

These relations demonstrate the physical similarity of the field dependencies for the magnetic properties in uniaxial ferromagnets and in easy-axis antiferromagnets near the SF field. This equivalence is established by introducing reduced units and a shift for the magnetization in Eq. (37), and by reduced units and a scale-factor for the susceptibility in Eq. (38). It is a consequence of the formal similarity in the phenomenological models Eqs. (17) and (24) for both systems. The relations Eqs. (37) and (38) are useful for comparative studies on reorientation transitions in uniaxial ferromagnets and antiferromagnets near the spin-flop.

C. Two-scale character of easy-axis antiferromagnets

The magnetic states analyzed in the previous two sections display the pronounced *two-scale* character of easy-axis antiferromagnets. The magnetic phase diagrams in Fig. 3 comprise the main features of the solutions in the spin-flop region. On the large scale of the (H_x, H_z) phase diagram two materials parameters rule the behaviour: the exchange or saturation field H_e and the SF field H_0 defined in Eqs. (3) and (7), respectively (Fig. 2). The former characterizes the strength of the antiferromagnetic exchange interaction, the latter comprises the interactions favouring easy-axis states. The equilibrium orientations of the staggered magnetization, derived from the Néel Eq. (9), result from the competition between these interactions and the applied field. Thus, the field H_0 sets the characteristic scale in the major part of the

magnetic phase diagram. Note, this is the only material parameter in the Néel equation (9).

In the vicinity of the SF field, where two of the main energy contributions cancel each other, much weaker (relativistic) interactions enter the scene set by Eq. (11). The characteristic scale in this region is given by the field H_c, as introduced in Eq. (16). Hence, $|H_c| \ll H_0$ defines a "fine" scale of the system. This scale gives the value of the potential barrier $\Delta w_0(H_{SF}) = H_c M_0$ at the spin-flop field and it fixes the size of the metastable regions around the field H_0, i.e. the astroids. The field $|H_c|$ includes two physically different contributions. One of them is the ratio between the sublattice second-order anisotropy K and the antiferromagnetic coupling. The other is the ratio between fourth- and second-order anisotropies, B_2 and B_1, of the staggered vector (see Eq. (5)). Generally, the two terms have same order of magnitude.

The strengths of the magnetic couplings in usual antiferromagnetic materials obey a well-defined hierarchy with very strong exchange and weaker uniaxial anisotropy. This hierarchy is given by the relations $J \gg K, K', B_1 \gg B_2$. Hence, the field $H_0 = H_e\sqrt{B_1/(2J)}$ is much smaller than the exchange field H_e, and $H_c = (K/J + B_2/B_1)H_0/2$ is much smaller than H_0. Correspondingly, the jump of the magnetization at the SF transition is small $\Delta m \sim H_0/H_e \ll 1$ (see Eqs. (27), (28)). The potential barrier separating the stable states at the SF field $\Delta w(H_{SF}) = \varkappa B_1 M_0^2$ is again much smaller than the barrier in the ground state, $\Delta w(0) = B_1 M_0^2$, and the region of the metastable states is restricted to a close vicinity of the SF field, $\Delta H \sim H_c$. This causes the unusually high sensitivity of the magnetic states near SF field with respect to small changes in strength and direction of applied fields. For example, in an antiferromagnet with $\varkappa > 0$ the rotation of the magnetic field $H = H_{SF}$ from $\psi = -\psi_c$ to $\psi = \psi_c$ causes a change of the staggered magnetization from $\theta = \pi/4$ to $\theta = -\pi/4$. This lability of the magnetic states is the underlying reason for the remarkable magnetic effects in the SF region.

IV. DEMAGNETIZATION EFFECTS AND MULTIDOMAIN STATES

In the previous section the equilibrium magnetic configurations have been derived as functions of the internal magnetic field $\mathbf{H}$, which differs from the applied *external* field $\mathbf{H}^{(e)}$ due to the demagnetization field $\mathbf{H}^{(m)}$ of the sample.[43] In a homogeneneously magnetized ellipsoidal sample (including the limiting cases, i.e. plates and long cylinders) the equation

$$\mathbf{H}^{(e)} = \mathbf{H} + 4\pi\widehat{\mathbf{N}}\mathbf{M}(\mathbf{H}), \tag{39}$$

establishes the relation between the external and internal magnetic fields. This relation allows to express the solutions for magnetic states as functions of the external field by using the demagnetization tensor $\widehat{\mathbf{N}}$ of the sample. However, the relation between internal and external fields breaks down at field-induced phase transitions.[10,43] In the vicinity of such transitions the homogeneous states are unstable with respect to the transformation into multidomain structures consisting of domains formed from the competing phases.[10,43] Within the *thermodynamic* approximation or generalized phase theory, two-phase multidomain states are described by the equation

$$\mathbf{H}^{(e)} = \mathbf{H}_{tr} + 4\pi\widehat{\mathbf{N}} < \mathbf{M} >, \tag{40}$$

where $\mathbf{H}_{tr}$ is the field value for the first-order transition.[10,43] Here, $< \mathbf{M} >= \xi_1\mathbf{M}^{(1)} + \xi_2\mathbf{M}^{(2)}$, $\mathbf{M}_i$ is the total average magnetization, and the variable parameters ξ_i are the volume fractions of the coexisting phases ($i = 1, 2$, $\xi_1 + \xi_2 = 1$). For the SF transition the phase theory approximation has been found to be valid practically in all regions of the phase diagram, where multidomain states exist.[10,16]

For model (15) with $\varkappa > 0$ the phase theory equations (40) can be written in the following form

$$\begin{aligned} H_x^{(e)} &= H_x\,(1 + \eta N_{xx}) \\ &\quad +\eta N_{xz}(\xi_1 - \xi_2)\sqrt{H_c^2 - H_x^2} + \eta N_{xz} H_c, \\ H_z^{(e)} &= H_{SF} + H_x\tilde{\eta}N_{xz} \\ &\quad +\eta N_{zz}(\xi_1 - \xi_2)\sqrt{H_c^2 - H_x^2} + \eta N_{zz} H_c\,, \end{aligned} \tag{41}$$

where H_x varies along the first-order transition line ($|H_x| \le H_c$, $H_z = H_{SF}$). The parameter $\eta = 2\pi M_{SF}/H_c = \pi/(\varkappa J)$ measures the ratio of the stray field energy and the potential barrier between the coexisting phases at the SF transition. Equations (41) allow us to derive the parameters of the multidomain states, H_x, ξ_i, as functions of the external field. In particular, for the relevant case with $N_{xz} = 0$, Eqs.(41) with $\xi_{1(2)} = 1$ yield the boundary of the multidomain states as an ellipse

$$1 = \left[\frac{H_x^{(e)}}{H_c + 2\pi N_{xx} M_{SF}}\right]^2 + \left[\frac{H_z^{(e)} - H_{SF} - 2\pi N_{zz} M_{SF}}{2\pi N_{zz} M_{SF}}\right]^2 \tag{42}$$

with semiaxes $a = H_c + 2\pi N_{xx} M_{SF}$, $b = 2\pi N_{zz} M_{SF}$ (Fig. 8(A)). For $\varkappa < 0$ similar equations yield the boundary ellipse

$$1 = \left[\frac{H_x^{(e)}}{2\pi N_{xx} M_{SF}}\right]^2 + \left[\frac{H_z^{(e)} - H_{SF} - 2\pi N_{zz} M_{SF}}{H_c + 2\pi N_{zz} M_{SF}}\right]^2 \tag{43}$$

with semiaxes $a = 2\pi N_{xx} M_{SF}$, $b = H_c + 2\pi N_{zz} M_{SF}$ (Fig. 8(B)).

The largest tilt angles between the applied field and the easy axis, at which the multidomain states still exist, can be readily derived from Eqs. (42), (43),

$$\begin{aligned} \psi_{cI}^{(e)} &= \frac{H_c + 2\pi N_{xx} M_{SF}}{H_{SF}} = \psi_c + \frac{\pi N_{xx}}{J} \text{ for } \varkappa > 0\,, \\ \psi_{cII}^{(e)} &= \frac{2\pi N_{xx} M_{SF}}{H_{SF}} = \frac{\pi N_{xx}}{J} \text{ for } \varkappa < 0\,. \end{aligned} \tag{44}$$

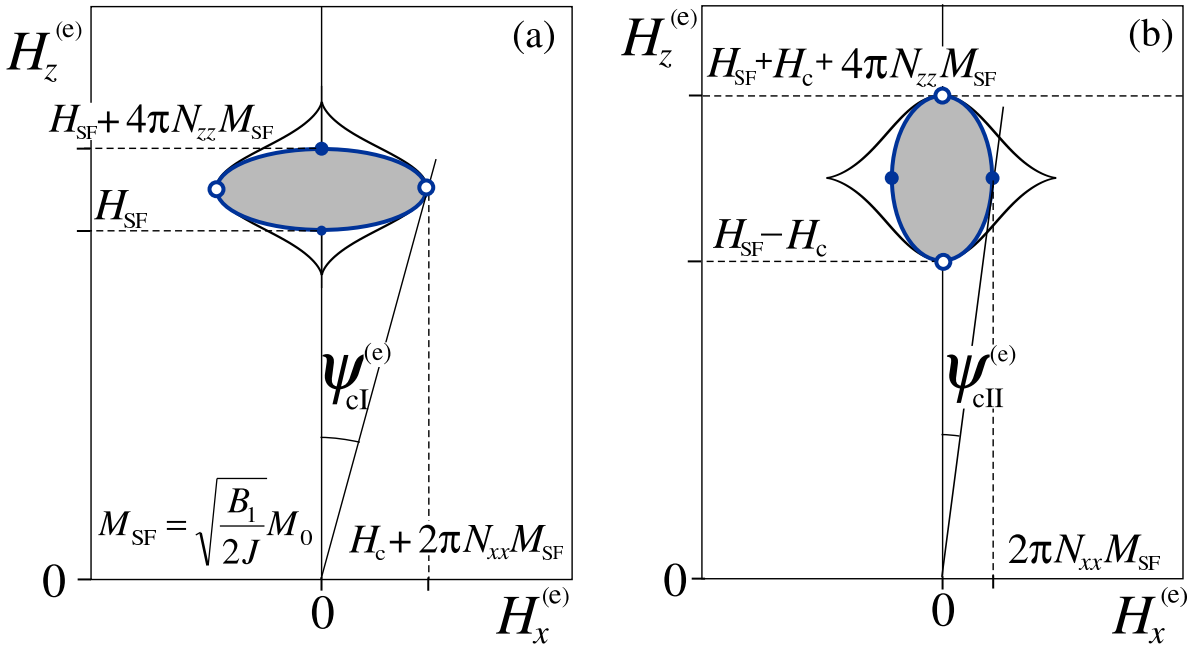

FIG. 8: Magnetic phase diagrams in components of the external field $(H_x^{(e)}, H_z^{(e)})$ for $\varkappa > 0$ (a) and $\varkappa < 0$ (b) include regions of the multidomain states (shaded areas).

The phase diagrams in Fig. 8 demonstrate the strong formal resemblance for the two qualitatively different cases. In both cases thermodynamically stable multidomain states arise near the SF transition in a close vicinity to the SF field. However, due to the different character of the phase transitions for $\varkappa > 0$ and $\varkappa < 0$, Eqs. (21) and 22), the evolution of the magnetic states within the multidomain regions (42) and (43) is different. For $\varkappa > 0$ the competing phases (21) coexist along the horizontal line segment ($H_z = H_{SF}$, $|H_x| \le H_c$). In the $(H_x^{(e)}, H_x^{(e)})$ phase plane a set of the vertical straight lines describes regions with these fixed transition fields (Fig. 8 (a)). Due to the smallness of $\psi_{cI}^{(e)}$ (44) external magnetic fields with fixed directions ($|\psi^{(e)}| \le \psi_{cI}^{(e)}$ practically intersect the region of the multidomain states (42) along the lines with a fixed transition field. A variation of fields with such a fixed orientation causes in the system magnetization processes through the displacement of domain walls between the coexisting states. On the other hand, rotating magnetic fields with fixed amplitude that cross the region (42) mainly cause a continuous deformation of the magnetic configurations within the domains. For $\varkappa < 0$ rotating fields cross the multidomain region (43) almost perfectly along lines corresponding to fixed internal fields. Thus, a rotating field induces a redistribution of the domains. On the other hand, magnetic fields with fixed directions produce mainly reorientation effects within the domains.

Correspondingly, the limiting angles (44) have a different physical meaning in both cases. For systems with $\varkappa > 0$ the critical points at $\psi^{(e)} = \pm\psi_{cI}^{(e)}$, $H^{(e)} = H_{SF}+2\pi N_{zz}M_{SF}$ correspond to internal states where the difference between the magnetic configurations in the coexisting phases disappears. For antiferromagnets with $\varkappa < 0$ the transition into the homogeneous state at the critical points $\psi^{(e)} = \pm\psi_{cII}^{(e)}$, $H^{(e)} = H_{SF}+2\pi N_{zz}M_{SF}$ occurs by a complete replacement of one of the coexisting phases by the other through domain processes.

The quantitative description of the magnetization in the multidomain states is provided by Eq. (40). This equation together with those for $\mathbf{M}(\mathbf{H})$ (27), (28) yields the functions $\langle\mathbf{M}\rangle(\mathbf{H}^{(e)})$. It follows from (40) that the magnetization is a linear functions of the applied field only when $\mathbf{H}^{(e)}$ varies along lines corresponding to fixed internal transition fields. In the general case the variation of the transition field $\mathbf{H}^{(t)}(\mathbf{H}^{(e)})$ causes complex dependencies of the magnetization on the external field in the multidomain state. Differentiation of $\langle\mathbf{M}\rangle$ in Eq. (40) yields the equation for the components of the magnetic susceptibility (cf. [10])

$$4\pi N_{ij}\chi_{jk} = \delta_{ik} - \frac{\partial H_i^{(t)}}{\partial H_k^{(e)}}\,. \qquad (45)$$

The first term on the right side of (45) describes the process of a redistribution of volume fractions for the different phases through *displacement of domain walls*, while the second term is associated with the variation of the magnetic states within the domains by *rotations of the magnetization*.

In homogeneous phases Eq. (39) allows one to relate the external susceptibility $\hat{\chi}^{(e)}$ and the internal suscepti-

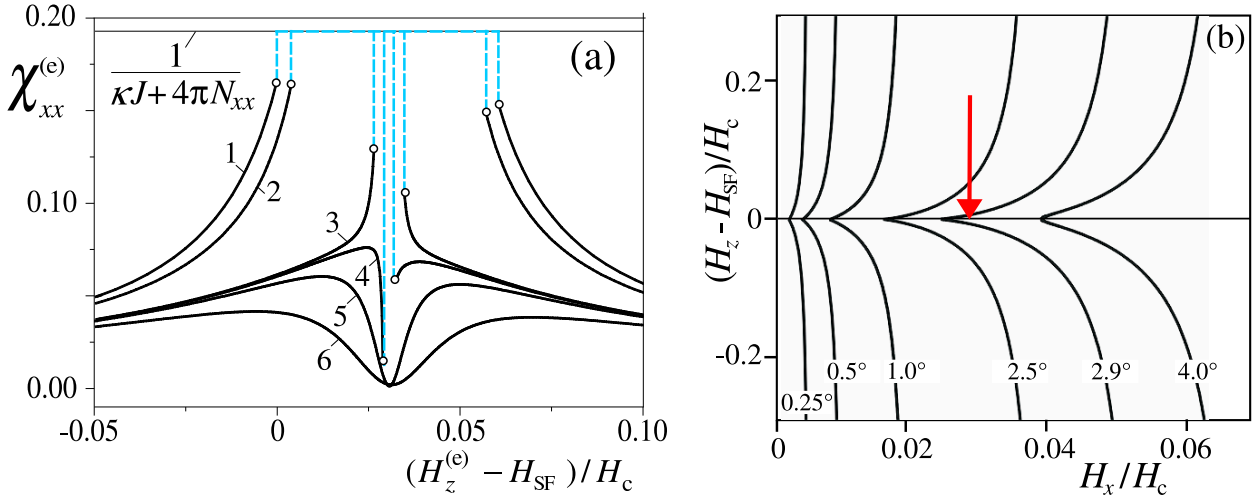

FIG. 9: Dependencies of $\chi^{(e)}_{xx}$ on external field calculated for $(C_2H_5NH_3)_2CuCl_4$ for different fixed values of $\psi^{(e)}$: $0.1°(1), 1.50°(2), 2.86°(3), 2.92°(4), 2.98°(5), 3.50°(6)$. Black solid lines correspond to the homogeneous phases and dashed (blue) lines to the multidomain states. Hollow points indicate the boundaries between these regions. Variations of the internal magnetic field $\mathbf{H}(H^{(e)})$ for fixed directions of the external field, $\psi^{(e)} = \text{const}$ (b). The (red) arrow in (b) indicates the location of the endpoint of first-order transition. The curved "trajectories" $H(H^{(e)}$ explain the reentrant character of the $\chi^{(e)}_{xx}(H^{(e)})$ functions in (a).

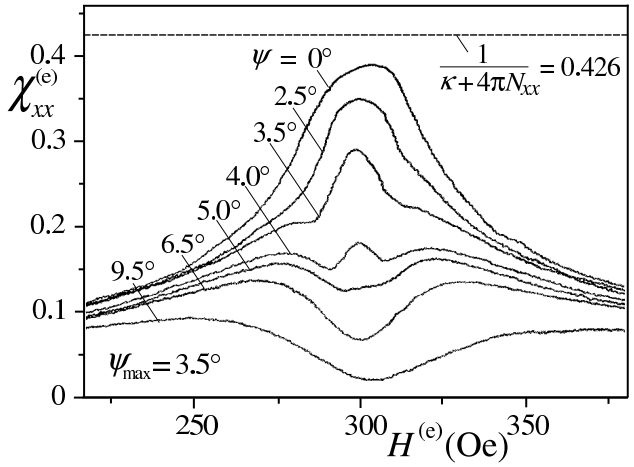

FIG. 10: Experimental dependencies of $\chi^{(e)}_{xx}$ on the external field $H^{(e)}$ for a number of fixed angles $\psi^{(e)}$ for a sphere of $(C_2H_5NH_3)_2$ $CuCl_4$ (Sample No. 1) at T = 4.2 K.

bility $\hat{\chi}$

$$\hat{\chi}^{(e)} = \left(\hat{\chi}^{-1} + 4\pi\hat{N}\right)^{-1}. \qquad (46)$$

Eqs. (40), (45), (46) transform the components of the net magnetization (24) and magnetic susceptibility (30), (31), (32) derived in the components of the internal field into those in components of the external field. The tensor of external susceptibility (46) includes the internal susceptibility $\hat{\chi}$ and the stray field contribution $\hat{\chi}_m = (4\pi\hat{N})^{-1}$ known as *shape susceptibility.*[10] In the multidomain state with fields varying along the lines of the fixed transition field the external susceptibility as given by (45) has only contributions from the shape susceptibility, $4\pi N_{ij}\chi_{jk} = \delta_{ik}$. When the evolution of a multidomain state involves a variation of the transition field a specific susceptibility contribution arises that is associated with the rotation of the magnetic states within in the domains. In particular, for the multidomain states in Fig. 8 along the line $H^{(e)}_x = 0$

$$\chi^{(e)}_{zz} = \frac{1}{4\pi N_{zz}} \quad (\varkappa > 0), \qquad (47)$$
$$\chi^{(e)}_{zz} = \frac{1}{4|\varkappa|J + 4\pi N_{zz}} \quad (\varkappa < 0).$$

For $\varkappa > 0$ the magnetic field varies along the line of the fixed transition field, and the susceptibility includes only shape contribution. For $\varkappa < 0$ the magnetic field varies along the line with fixed volume fractions, $\xi_1 = \xi_2 = 1/2$, and the evolution of the system consists of a continuous reorientation in the domains (22). For this process the net magnetization is derived from Eq. (28), and the internal susceptibility is $\chi_{zz} = 1/(4|\varkappa|J)$. The external susceptibility $\chi^{(e)}_{zz}$ (47) includes both internal and shape contributions. Generally during the SF transition the values of the internal susceptibility $1/(|\varkappa|J)$ (30), (31), (32) arising due to variation of the homogeneous magnetic states and the shape susceptiblity $1/N$ originating from the reconstruction of the multidomain states are of the same order and larger than the values for the external susceptibility outside of the SF region. For example, in the external field along the easy axis $\chi^{(e)}$ equals zero in the AF phase, and in the SF phase $\chi^{(e)}_{zz} = 1/(2J+4\pi N_{zz})$.

Fig. 9 (a) shows the calculated external-field dependencies of $\chi_{xx}(H^{(e)})$ for a number of fixed angles $\psi^{(e)}$ and with materials parameters close to those for

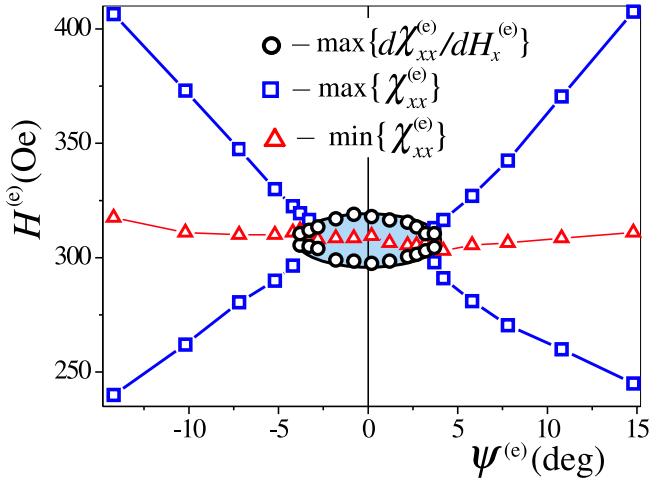

FIG. 11: Location of extremal points of $\chi^{(e)}_{xx}$ and $\partial\chi^{(e)}_{xx}/\partial H^{(e)}$ in the phase plane $(H^{(e)}, \psi^{(e)})$ for an elliptical $(C_2H_5NH_3)_2$ $CuCl_4$ sample (No. 3). The shaded area indicates the region of multidomain states.

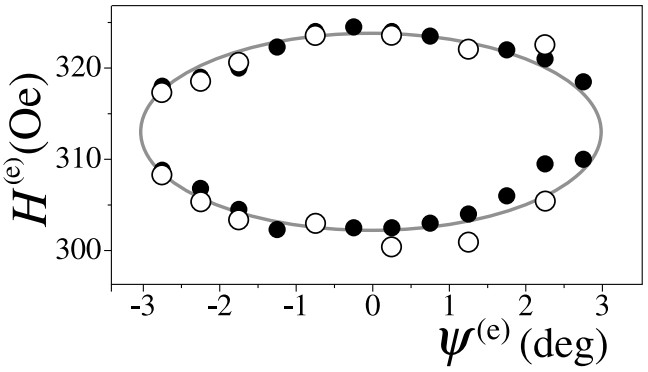

FIG. 12: Experimental phase diagram in components of applied field for $(C_2H_5NH_3)_2$ $CuCl_4$ (for spherical and ellipsoidal samples). The region of multidomain states is within the area circumscribed by measured points. Filled circles give the field values for the maxima in $\partial\chi_{xz}/\partial H^{(e)}_z(H^{(e)}_z)$; hollow circles give the inflection points in $\partial\chi_{zz}/\partial H^{(e)}_z(H^{(e)}_z)$.

$(C_2H_5NH_3)_2CuCl_4$. According to previous investigations in this antiferromagnet, $\varkappa > 0$.[20,49] The functions $\chi_{xx}(H^{(e)})$ for small angles $\psi^{(e)} < \psi^{(e)}_{cI}$, are given by *lines 1-3* in Fig. 9 (a). They cross field-dependent regions corresponding to homogeneous phases (black solid lines) and areas with constant susceptibilities (dashed blue lines) indicating multidomain regions. For $\psi^{(e)} < \psi^{(e)}_{cI}$ the functions $\chi_{xx}(H^{(e)})$ (*lines 5, 6*) have characteristic features as described in the previous section (Figs. 5 and Eqs. (33), (34)). The intermediate *line 4* shows ambivalent features. In the center it includes a jump into the multidomain states as the lines for $\psi^{(e)} < \psi^{(e)}_{cI}$, but outside this narrow central feature the function $\chi_{xx}(H^{(e)}$ behaves similar to those for $\psi^{(e)} > \psi^{(e)}_{cI}$. This interesting effect is explained by strong deviations of the total magnetization from the easy axis in the vicinity of SF field. The enhanced values of the tranverse magnetization M_x (Fig. 4 (c)) create a strong demagnetization screening near the SF field. Accordingly, for the external field varying along lines $\psi^{(e)} = const$, interal field "trajectories" $H(H^{(e)})$ deviate towards the H_z axis near the SF field, as depicted in Fig. 9 (b). The trajectory for the evolution of the internal field **H** starts from outside the transition region i.e. $|H_x| > H_c$ but enters this area in the vicinity of the SF field for the external field applied under an angle $\psi^{(e)} = 2°$.

V. MAGNETIC PHASE DIAGRAM OF $(C_2H_5NH_3)_2CUCL_4$

An experimental investigations of the differential magnetic susceptibility was carried out for $(C_2H_5NH_3)_2CuCl_4$.[47] This model antiferromagnet has orthorhombic lattice structure with space group is Pbca, and orders at a Néel temperature $T_N = 10.20$ K.[8]. The magnetic structure consists of ferromagnetic layers parallel to the $x0z$ planes in the notation of this paper with weak antiferromagnetic couplings. According to Ref. [8] the ferromagnetic intra-layer interactions corresponds to an effective field 500 kOe, while antiferromagnetic coupling between layers is $JM_0 = 837.5$ Oe. A weak second-order anisotropy in the $x0z$ plane $KM_0 =$ 76 Oe stabilizes the collinear ground state with the sublattice magnetizations $\mathbf{M}_i$ along the z-axis. At T = 4.2 K the spin-flop field is at $H_{SF} = 305$ Oe. Magnetic interactions in $(C_2H_5NH_3)_2CuCl_4$ include a Dzyaloshinsky-Moriya coupling described by an energy contribution $w_D = D(M_{1x}M_{2y} - M_{2x}M_{1y})$ with an effective field DM_0= 119 Oe.[8] Generally this interaction rotates the magnetization vectors $\mathbf{M}_i$ away from the basal plane $x0z$. However, due to the strong orthorhombic anisotropy with a value of 1504 Oe, the vectors $\mathbf{M}_i$ are practically confined to the basal plane. Deviations from this plane do not exceed 2°.[20] Thus, the planar model (11) can be applied to this antiferromagnet.

The differential magnetic susceptibility components were measured with an inductive technique using three pairs of modulating and pick-up coils arranged along perpendicular directions. The modulating fields had amplitudes between 0.3 and 1.0 Oe at frequencies of 9, 17-21, 86 and 133 Hz. The three samples used for the measurements were cut from a $(C_2H_5NH_3)_2CuCl_4$ single crystal. The samples had the following geometrical parameters: (Sample No. 1) a sphere with diameter 3.1 mm ($N_{xx} = N_{zz} = 1/3$); (Sample No. 2) an ellipsoid with axes $a_x = 5.00$ mm, $a_y = 1.75$ mm, $a_z = 5.00$ mm (N_{xx} =0.185, $N_{zz} = 0.185$); (Sample No. 3) an ellipsoid with $a_x = 3.43$ mm, $a_y = 2.45$ mm, $a_z = 5.75$ mm (N_{xx} =0.344, $N_{zz} = 0.186$). All the measurements of components $\chi^{(e)}_{ij}$ have been carried out at $T = 4.2$ K. The recorded data for all investigated samples are in

close accordance with the theoretical results expounded in previous sections. An example is shown in Fig. (10), where $\chi_{xx}^{(\mathrm{e})}$ components are plotted for the spherical sample. The experimental data follow closely the theoretical results of Eq. (30) as sketched in Fig. 9. In particular, the dependencies of $\chi_{xx}^{(\mathrm{e})}(H^{(\mathrm{e})})$ for $\psi^{(\mathrm{e})} = 3.5°, 4.0°$ and $5°$ display the reentrant behaviour imposed by the rotation of the internal field towards the H_z-axis, as demonstrated in Fig. 9. By fitting experimental data for the $\chi_{ij}^{(\mathrm{e})}$ components and their field derivatives with the theoretical dependencies, values of the material parameters can be deduced and the magnetic phase diagram of this antiferromagnet has been constructed. Fig. 11 shows the locations of the extremal points for $\chi_{xx}^{(\mathrm{e})}$ and $d\chi_{xx}^{(\mathrm{e})}/dH^{(\mathrm{e})}$ and the region of the multidomain states in the $(H^{(\mathrm{e})}, \psi^{(\mathrm{e})})$ phase diagram of the ellipsoidal samples.

The experimental $(H^{(\mathrm{e})}, \psi^{(\mathrm{e})})$ phase diagram for the spherical sample is shown in Fig. 12. In particular, for the maximal angle $\psi_{\mathrm{cI}}^{(\mathrm{e})}$ the following results have been obtained (spherical sample No. 1) $3.50° \pm 0.65°$ (sample No. 2) $2.70° \pm 0.45°$ (sample No. 3) $3.55° \pm 0.65°$ These results yield the values of the spin-flop field $H_{\mathrm{SF}} = 306$ Oe, the critical angle $\psi_{\mathrm{c}} = 1.7°$, and the characteristic fields $H_0 = 300$ Oe and $H_{\mathrm{c}} = 9.1$ Oe.

VI. CONCLUSIONS

Magnetic configurations for an extended class of two-sublattice collinear easy-axis antiferromagnets have been obtained as functions of the values and directions of the applied magnetic field, and the corresponding magnetic phase diagrams have been constructed. The magnetic behaviour of these materials strongly depends on the strengths of the applied field. In the main part of the magnetic phase diagram they are described by the well-known Néel model (6). In the vicinity of the SF field they are described by an effective model for a reorientation transition that is formally equivalent to the Stoner-Wohlfarth model of a uniaxial ferromagnet (15). This *two-scale* character of easy-axis antiferromagnets has been ignored in most previous investigations. The analysis of magnetic-field-driven reorientation effects and the concomitant multidomain states provides a consistent picture of the magnetization processes near the SF transition. At the SF transition the weak intrinsic higher-order couplings of the antiferromagnetic material and the dipolar stray field cause important and noticeable effects and must be included in the analysis. These effects are responsible for the prominent anomalies in the magnetization curves and the magnetic susceptibilities of antiferromagnets in the spin-flop region. The anomalies provide effective approaches for investigations on magnetic properties of antiferromagnets that are usually hidden away from the spin-flop region. The validity of this approach has been demonstrated by an application to an orthorhombic antiferromagnet.

The results on bulk antiferromagnets may also be extended to confined antiferromagnetic systems by including surface/interface-induced interactions into the phenomenological models. In Ref. [50] it was shown that the interplay between surface-induced and intrinsic magnetic interactions yield a rich variety of specific magnetic states including spatially inhomogeneous twisted states in the vicinity of the SF field. The further development the theory for such cases will be important for an understanding of the magnetization processes in ferro/antiferromagnetic bilayers,[34,37,41] and in antiferromagnetic nanoparticles.[33]

The phenomenological model of the two-sublattice antiferromagnet (1) and its variants can be adopted also to describe magnetic states in synthetic antiferromagnets.[38,39]

Acknowledgments

This work was financially supported by DFG through SPP 1133, project RO 2238/6-1. A. N. B. thanks H. Eschrig for support and hospitality at the IFW Dresden.

* Electronic address: a.bogdanov@ifw-dresden.de
† Electronic address: u.roessler@ifw-dresden.de

[1] L. Néel, Ann. de Physique **5**, 232 (1936); Proc. Phys. Soc. (London) A **65**, 869 (1952).
[2] N. J. Poulis, J. van den Handel, J. Ubbink, J. A. Poulis, C. J. Gorter, Phys. Rev. **82**, 552 (1951).
[3] The term "spin-flop" has been used since the early 1950s. See, e.g., J. Ubbink, J. A. Poulis, H. J. Gerritsen, C. J. Gorter, Physica **19**, 928 (1953).
[4] N. J. Poulis, G. E G. Hardeman, Physica **18**, 201 (1952); Physica **20**, 7 (1954); C. J. Gorter, Rev. Mod. Phys. **25**, 332 (1953).
[5] Y. Shapira, J. Zak, Phys. Rev. **170**, 503 (1968); Y. Shapira, S. Foner, Phys. Rev. B **1**, 3083 (1970).
[6] K. W. Blazey, H. Rohrer, Phys. Rev. **173**, 574 (1968); K. W. Blazey, H. Rohrer, R. Webster, Phys. Rev. B **4**, 2287 (1971).
[7] S. Foner, Phys. Rev. **130**, 183 (1963); Y. Shapira, Phys. Rev. **187**, 734 (1969); J. W. Allen, Phys. Rev. B **7**, 4915 (1973).
[8] L. J. de Jongh, W. D. van Amstel, A. R. Miedema, Physica **58**, 277 (1972).
[9] J. E. Rives, Phys. Rev. **162**, 491 (1967); C. C. Becerra, N. F. Oliveira, Jr., A. Paduan-Filho, W. Figueiredo, M. V. P. Souza, Phys. Rev. B **38**, 6887 (1988).
[10] V. G. Baryakhtar, A. N. Bogdanov, D. A. Yablonskii, Usp. Fiz. Nauk **156**, 47 (1988) [Sov. Phys. Usp. **31**, 810 (1988)].
[11] A. N. Bogdanov, U. K. Rößler, M. Wolf, K.-H. Müller, Phys. Rev. B **66**, 214410 (2002).
[12] A.N. Bogdanov, Sov. J. Low Temp. Phys. **12**, 290 (1986).

[13] M. A. Kastner, R. J. Birgeneau, G. Shirane, Y. Endoh, Rev. Mod. Phys. **70**, 897 (1998).

[14] I. Tsukada, J. Takeya, T. Masuda, K. Uchinokura, Phys. Rev. Lett. **87**, 127203 (2001).

[15] G. K. Chepurnykh, Fiz. Tverd. Tela **10**, 1917 (1968); H. Rohrer, H. Thomas, J. Appl. Phys. **40**, 1025 (1969).

[16] A. N. Bogdanov, V. T. Telepa, Fiz. Tverd. Tela **24**, 2420 (1982) [Sov. Phys. Solid State **24**, 1374 (1982)]; V. G. Baryakhtar, A. N. Bogdanov, V. T. Telepa, D. A. Yablonskii, Fiz. Tverd. Tela **26**, 389 (1984) [Sov. Phys. Solid State **26**, 231 (1984)]; V. G. Baryakhtar, A. N. Bogdanov, D. A. Yablonskii, Ukr. Fiz. Zh. **31**, 266 (1986).

[17] A. F. G. Wyatt, J. Phys C: Solid State **1**, 684 (1968); V. G. Baryakhtar, A. E. Borovik, V. A. Popov, JETP Lett. **9**, 391 (1969).

[18] K. L. Dudko, V. V. Eremenko, V. M. Fridman, Sov. Phys. JETP **34**, 362 (1972); *ibid.* **34**, 828 (1972); A. R. King, D. Paquette, Phys. Rev. Lett. **30**, 662 (1973); V. V. Yeremenko, A. V. Klichko, V. M. Naumenko, Zh. Eksp. Teor. Fiz. **89**, 1002 (1985).

[19] H. Rohrer, AIP Conference Proceedings **24**, 268 (1975); V. V. Eremenko, A. V. Klochko, V. N. Naumenko, V. V. Pishko, JETP Lett. **40**, 986 (1984).

[20] A. N. Bogdanov, A. V. Zhuravlev, A. I. Puzynya, Fiz. Nizk. Temp. **15**, 181 (1989).

[21] I. S. Jacobs, P. E. Lawrence, Phys. Rev. **164**, 866 (1967); A. I. Mitsek, P. F. Gaidanskii, V. N. Pushkar, phys. stat. sol. **38**, 69 (1970).

[22] D. L. Mills, Phys. Rev. Lett. **20**, 18 (1968); F. Keffer, H. Chow, Phys. Rev. Lett. **31**, 1061 (1973).

[23] P.-z. Wong, J. W. Cable, Phys. Rev. B **30**, 485 (1984).

[24] R. Lai, A. J. Sievers, Phys. Rev. Lett. **81**, 1937 (1998); U. T. Schwarz, L. Q. English, A. J. Sievers, Phys. Rev. Lett. **83**, 223 (1999); M. Sato, L. Q. English, B. E. Hubbard, A. J. Sievers, J. Appl. Phys. **91**, 8676 (2002).

[25] H. J. Mikeska, M. Steiner, Adv. Phys. **40**, 191 (1991); M. Fiebig, D. Fröhlich, R. V. Pisarev, J. App. Phys. **81**, 4875 (1997).

[26] M. E. Fisher, Phys. Rev. Lett. **34**, 1634 (1975); H. Rohrer, Phys. Rev. Lett. **34**, 1638 (1975); Y. Shapira, C. C. Becerra, Phys. Rev. B **16**, 4920 (1977); A. R. King, H. Rohrer, Phys. Rev. B **19**, 5864 (1979).

[27] T. Fries, Y. Shapira, F. Palacio, M. C. Morón, G. J. McIntyre, R. Kershaw, A. Wold, E. J. McNiff Jr., Phys. Rev. B **56**, 5424 (1997); M. Quintero, R. Cadenas, R. Tovar, E. Quintero, J. Gonzalez, J. Ruiz, J.C. Woolley, G. Lamarche, A.M. Lamarche, J.M. Broto, H. Rakoto, R. Barbaste, Physica B **294**, 471 (2001).

[28] W. Wernsdorfer, N. Aliaga-Alcalde, D. N. Hendrickson, G. Christou, Nature **416**, 406 (2002).

[29] A. Zheludev, S. Maslov, G. Shirane, Y. Sasago, N. Koide, K. Uchinokura, Phys. Rev. Lett. **78**, 4857 (1997); M.D. Lumsden, B.C. Sales, D. Mandrus, S.E. Nagler, J.R. Thompson, Phys. Rev. Lett. **86**, 159 (2001).

[30] M. R. Fitzsimmons, P. Yashar, C. Leighton, I. K. Schuller, J. Nogués C. F. Majkrzak J. A. Dura, Phys. Rev. Lett. **84**, 3986 (2000); C. Leighton, M. R. Fitzsimmons, P. Yashar, A. Hoffmann A, J. Nogués, J. Dura, C.F. Majkrzak, I.K. Schuller, Phys. Rev. Lett. **86**, 4394 (2001).

[31] E. E. Fullerton, D. T. Margulies, N. Supper, H. Do, M. Schabes, A. Berger, A. Moser, IEEE Trans. Mag. **39**, 639 (2003); A. Moser, K. Takano, D.T. Margulies, M. Albrecht, Y. Sonobe, Y. Ikeda, S.H. Sun, E.E. Fullerton, J. Phys. D **35**, R157 (2002).

[32] T. M. Maffitt, J. K. DeBrosse, J. A. Gabric, E. T. Gow, M. C. Lomorey, J. S. Parenteau, D. R. Willmott, M. A. Wood, W. J. Gallagher, IBM. J. Res. & Dev. **50**, 25 (2006).

[33] M. F. Hansen, C. B. Koch, S. Mørup, Phys. Rev. B **62**, 1124 (2000); H. Mamiya, I. Nakatani, T. Furubayashi, Phys. Rev. Lett. **88**, 067202 (2002); M. Bañobre-López, C. Vázquez-Vázquez, J. Rivas, M. A. López-Quintela, Nanotechnology **14**, 318 (2003).

[34] J. Nogués, I. K. Schuller, J. Magn. Magn. Mater. **192**, 203 (1999); S. Maat, K. Takano, S S. P. Parkin, E. E. Fullerton, Phys. Rev. Lett. **87**, 087202 (2001).

[35] R. W. Wang, D. L. Mills, E. E. Fullerton, J. E. Mattson, S. D. Bader, Phys. Rev. Lett. **72**, 920 (1994); S. G. E. te Velthuis, J. S. Jiang, S. D. Bader, G.P. Felcher, Phys. Rev. Lett. **89**, 127203 (2002).

[36] F. Nolting et al., Nature **405**, 767 (2000).

[37] J. Nogués, L. Morellon, C. Leighton, M. R. Ibarra, I. K. Schuller, Phys. Rev. B. **61**, R6455 (2000).

[38] D. C. Worledge, Appl. Phys. Lett. **84**, 2847 (2004); IBM. J. Res. & Dev. **50**, 69 (2006).

[39] A. N. Bogdanov, U. K. Rößler, Appl. Phys. Lett., in press (2006).

[40] U. K. Rößler, A. N. Bogdanov, Phys. Rev. B **69**, 094405 (2004); *ibid.* **69**, 184420 (2004); phys. stat. sol. (c) **1**, 3297 (2004).

[41] G. P. Felcher, R. Kleb, Europhys. Lett. **36**, 455 (1996).

[42] B. Stahl, E. Kankeleit, R. Gellert, M. Müller, A. Kamzin, Phys. Rev. Lett. **84**, 5632 (2000); B. Stahl, S. Bhattacharya, S. Gottschalk, J. Ellrich, H. Schmitt, J. Ebert, M. Ghafari, H. Hahn, A. Kamzin, D. Vcherashniy, A.R. Raju, Phys. Rev. B. **66**, 104426 (2002).

[43] A. Hubert, R. Schäfer, *Magnetic Domains. The Analysis of Magnetic Microstructures*, Springer, Berlin, 1998.

[44] E. A. Turov, *Physical Properties of Magnetically Ordered Crystals*, Academic Press, New York and London 1965; L. D. Landau, E. M. Lifshitz, *Statistical Physics. Course of Theoretical Physics*, Vol. V, Pergamon, Oxford, 1997.

[45] F. B. Anderson, H. B. Callen, Phys. Rev. **136**, A1068 (1964); J. Feder, E. Pytte, Phys. Rev. **168**, 640 (1968).

[46] A. I. Mitsek, N. P. Kolmakova, P. F. Gaidanskii, Fiz. Tverd. Tela **11**, 1258 (1969) [Sov. Phys. Solid State **11**, 1021 (1969)]; V. G. Baryakhtar, Pis'ma Zh. Eksp. Teor. Fiz. **30**, 654 (1979) [Sov. Phys. JETP Lett. **30**, 619 (1979)].

[47] Details of the experiments and data analysis will be presented elsewhere, A. V. Zhuravlev, U.K. Rößler, A. N. Bogdanov, to be published.

[48] E. C. Stoner, E. P. Wohlfarth, Phil. Trans. Roy. Soc. (London) A **240**, 599 (1948).

[49] A. N. Bogdanov, A. V. Zhuravlev, I. V. Zhikharev, U.K. Rößler, J. Magn. Magn. Mater. **290-291** 768 (2005).

[50] A. N. Bogdanov, U. K. Rößler, Phys. Rev. B **68**, 012407 (2003).